

Interaction and Fragmentation of Pulsed Laser Induced Microbubbles in a Narrow Gap

Yen-Hong Chen, Hong-Yu Chu, and Lin I

Department of Physics and Center for Complex Systems, National Central University, Chungli, Taiwan 32054, Republic of China
(Received 25 April 2005; published 27 January 2006)

We investigate the interaction dynamics of an existing stable microbubble B_1 and another laser induced nearby expanding microbubble B_2 in a thin ink sheet between two glass slices. The fast expanding B_2 causes anisotropic compression of B_1 with a forward penetrating jet. In the subsequent expansion stage of B_1 , the gas associated with jet protrusion to the opposite edge of B_1 and the nonuniform surrounding flow field induce necking with transverse inward jetting from the side lobes, which further interact with the axial jet and lead to the final fragmentation into smaller bubbles. At small interbubble distance, the backward interaction from B_1 first leads to the pointed pole of the expanding B_2 and then a backward jetting during its collapsing. The strong interaction can merge the two bubbles with complicated asymmetric intermediated patterns.

DOI: [10.1103/PhysRevLett.96.034505](https://doi.org/10.1103/PhysRevLett.96.034505)

PACS numbers: 47.55.dp, 47.20.Ma

The physics of bubbles, cavities, or 3D pulse-type spatial structures in extended media are interesting nonlinear problems [1–9]. The sound emission [3], bubble luminescence [4], and jet formation [5–9] in a bubble collapsing or under shock impact are the few well studied examples. In liquids, cavitation bubbles can be formed under tensile stress or sudden deposition of energy. In microsurgery of cellular structures and opening of or delivery through cell membrane, pulsed laser micro-beams are often used [10,11]. Microbubbles can be easily generated and interact with each other through the associated flow field. For example, the flow field accompanied by sudden bubble expansion can induce an interesting dynamical response on other existing bubbles nearby. The understanding of the interaction dynamics is important both for fundamental research and applications. In this work, this issue in a thin ink sheet is addressed using pulsed laser microbeams and time resolved digital microimaging under the precise control of the initial conditions of bubbles.

Usually, during the collapse of a bubble, a pressure gradient by the presence of a nearby boundary or a shock causes the formation of a jet [5–9]. For example, in the previous study, jetting and fragmentation of a 3D bubble into two smaller bubbles under the shock from an ultrasonic drive were reported [9]. In our system, under the flow generated by the sudden finite expansion of the microbubble B_2 induced by a laser pulse, it is not hard to imagine that the nearby existing stable bubble B_1 will be compressed with a forward jet, and then reexpand while the shock fades away. However, very little is known about the detailed interaction dynamics between two microbubbles, especially, the anisotropic reexpansion associated with the complicated fragmentation process of B_1 , and its backward impact on the expanding and then collapsing dynamics of B_2 . In this work, the above issues are explored under different laser energies and bubble separations.

The experimental system consists of the liquid cell, the pulse laser system for bubble and shock wave generation, and the microimaging system as depicted in Fig. 1. A

pulsed Nd:YAG laser ($\lambda = 532$ nm and 10 ns pulse width) is aligned and focused on a thin blue ink sheet (water-based inkjet ink, HPI-8449 C, InkTec Co., for Hewlett Packard printers) sandwiched between two horizontal glass slices at 10 μm gap width, through the objective lens (10 \times and numerical aperture = 0.3) of the microscope to generate bubbles. The viscosity and compressibility of the ink are similar to water. The buoyancy effect on bubbles can be avoided. When B_1 generated by the first laser pulse (energy fixed at 220 μJ for all the runs in this Letter) reaches the final stable state (it can maintain 170 μm in diameter in 1 min), the digitally controlled microstage (with 0.3 μm precision) is shifted horizontally for the generation of B_2 by the second laser pulse. Because of the precise controls of the energies (E_1 and E_2) of and the distance (D_L) between the two successive laser pulses, the initial condition of the experiment and the first compression stage of B_1 are highly reproducible (less than 3% fluctuation). By gradually shifting the triggering time of a gated and intensified CCD (ICCD) mounted on top of the microscope, the dynamical evolutions of both bubbles after the second laser pulse are studied in detail. A white light emitting diode mounted below the liquid cell is used for illumination. The gating time of the ICCD is fixed at 1 μs .

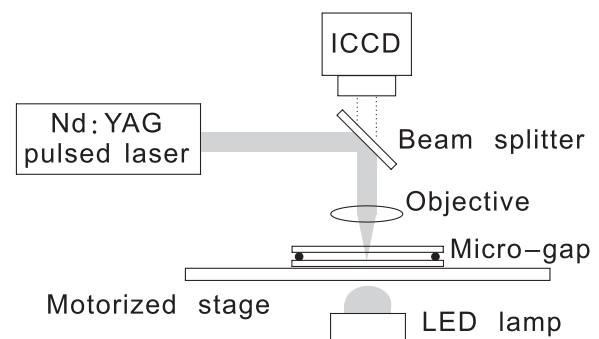


FIG. 1. The side view of the experimental set up.

The sequential shadow graphs in Fig. 2 show the bubble evolution at $E_1 = 220 \mu\text{J}$ and $E_2 = 90 \mu\text{J}$, and $D_L = 500 \mu\text{m}$. The second laser pulse is fired at $t = 0$ s. Figure 3(a) shows the time evolution of the volumes (by digitally measuring the areas of the bubbles from CCD pictures) of B_1 and B_2 (normalized to the initial volume of B_1). Initially the pressure perturbation travels at about 900 m/s and reaches the left edge of B_1 in $0.5 \mu\text{s}$ (not shown). Stages I–III in Fig. 3(a) represent the sequential compression, reexpansion, and the final contraction stages of B_1 respectively. In stage I, the incidence of the pressure wave causes the compression of B_1 with a rightward axial jet, while the right edge of B_1 remains unperturbed. At $t = 6 \mu\text{s}$, the jet hits the right edge of B_1 and splits B_1 into two symmetric parts. The volume also reaches the minimum. After that, the expansion process begins. A butterfly-shape pattern with two symmetric side lobes is observed associated with the deeper protrusion of the jet into the liquid beyond the right edge of B_1 , where the necking occurs. The

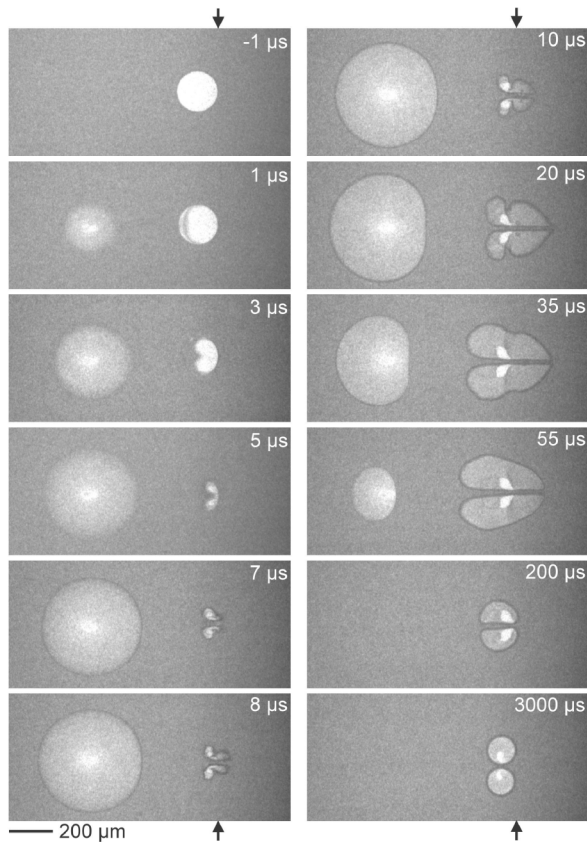


FIG. 2. The sequential snap shots showing the compression, reexpansion, and shrinking of B_1 with jet formation and fragmentation under the interaction from B_2 (the left bubble) at $E_1 = 220 \mu\text{J}$, $E_2 = 90 \mu\text{J}$ and $D_L = 500 \mu\text{m}$. B_2 is generated at $t = 0 \mu\text{s}$. The arrows indicate the location of the initial right edge of B_1 . The bright areas in B_1 after $8 \mu\text{s}$ correspond to the smallest compressed area in the entire process, where the glass has never been wetted. They allow the best transmission of the illuminating light.

necking gradually becomes less obvious and disappears in the expansion process. In stage III (after $45 \mu\text{s}$), the two kidney shaped lobes start to contract again, and evolve to the two final stable circular bubbles. The sketches in Fig. 3(b) show the bubble shape evolution for the three different stages. Figure 3(c) shows that increasing E_2 decreases (increases) the minimum (maximum) volume of B_1 at the end of stage I (II).

The sudden expansion of the second bubble generates a gradient pressure field. Even though the gap is very narrow, the viscosity and the capillary force effects are not dominant because of the high Reynolds number ($\text{Re} \sim 1000$) and Weber number ($\text{We} \sim 5000$) under the large inertia induced by the high speed process in the first $10 \mu\text{s}$. Similar generic behaviors are found as the gap width increases by 3 times. Based on the theory of the Richtmyer-Meshkov instability [12] and the axial symmetry of the two interacting bubble, the observed compression and the axial jet formation in stage I are consequences of inertia and the pressure wave-induced anisotropic liquid flow, which amplifies the perturbed gas-liquid interface without restoring mechanism. Similar axial jetting has also been observed in the collapsing stage of the 3D bubble under the shock from an ultrasonic drive [9]. The jetting is the major cause for the initial bubble fragmentation. The pressure of the surrounding liquid for B_1 gradually drops due to the finite

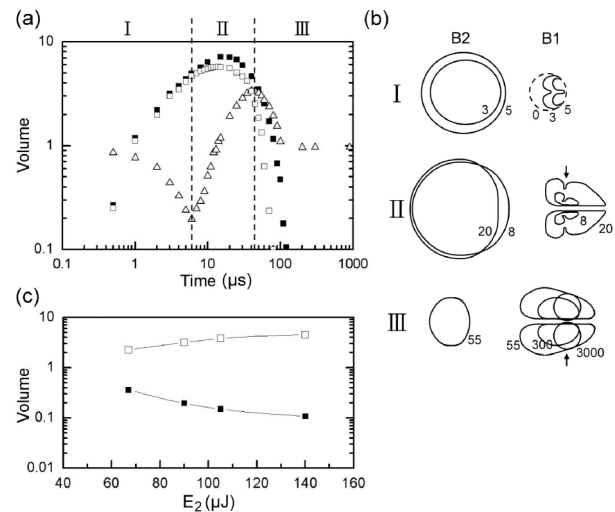


FIG. 3. (a) The temporal evolution of the volumes (normalized by the initial volume of B_1) of B_1 (open triangles) and B_2 (open squares) at the same condition as in Fig. 2. Stages I–III correspond to the compression, reexpansion, and final contraction stages of B_1 . The solid squares show the volume evolution of B_2 under the same E_2 but in the absence of B_1 . (b) The sketches for the bubble shape evolution in the three stages I–III for the run shown in Fig. 2. The units of the numbers are μs . The arrows indicate the position of the initial right edge of B_1 , where the transverse necking occurs. (c) The minimum compression (solid square) and the maximum expansion (open square) volumes of B_1 (normalized to the initial volume of B_1) at different E_2 .

laser energy. The inertia of the surrounding liquid over-compresses B_1 . The interplay of the accumulated high pressure in B_1 and the low pressure in the trough following the pressure wave from B_2 leads to the reexpanding stage II. Similar to the cavity formation associated with a falling liquid column crossing a gas-liquid interface [13], some gas goes along with the jet when it protrudes through the opposite gas-liquid interface (see the $7 \mu\text{s}$ picture in Fig. 2). Along with the nonuniform surrounding flow and pressure fields, the transverse necking at the initial right edges of B_1 is induced and the butterfly-shaped side lobes are formed [6]. Namely, the transverse necking region has the highest pressure and is the hardest region to deform compared to the low pressure regions downstream. Once the high pressure expanding gas entrained with the axial gas goes beyond the transverse necking region, it has a faster expansion, which causes the formation of the butterfly shape in the expanding stage II. The expansion of B_1 reduces its internal pressure and also over-compresses the surrounding liquid due to the similar inertia effect, which leads to the final compression stage III.

What will happen when the interaction becomes stronger by increasing E_2 or decreasing D_L ? Figures 4(a)–4(d) show a few sets of typical snapshots of B_1 as E_2 increases to $105 \mu\text{J}$ but the same E_1 and D_L as the run in Fig. 2. At increased E_2 , the general behaviors of the initial compression and jetting (until the jet reaches the right boundary of B_1) in stage I remain similar, but the stronger pressure wave speeds up the compression [Fig. 4(a)]. In stage II, the transverse inward jet in the transverse necking region becomes quite unstable [see the examples of the intermediate and the corresponding final stages under the same initial condition in Figs. 4(b)–4(d)]. Sometimes it directly mixes with the axial jet and breaks the necking. Sometimes it bifurcates with one branch turning rightward and even outward again, which leads to the further fragmentation of that lobe into more than two final leaves. The instability makes the entire fragmentation pattern quite complicated and asymmetric. The fragmented small bubble travels at speeds of about 1 mm/s . Figure 4(e) shows that decreasing D_L to $350 \mu\text{m}$ makes the fragmentation pattern more complicated because of the increase of the compression strength and the change of geometrical relation between B_1 and B_2 . Figure 4(f) shows that, unlike the intuitive expectation, further increasing E_2 to $140 \mu\text{J}$ while increasing D_L back to $500 \mu\text{m}$ does not lead to the complicated fragmentation pattern of B_1 . The leftward expansion of B_1 (the part left to the initial right edge of B_1) is fully suppressed such that the transverse necking disappears in stage II. B_1 is mainly split into two major symmetric parts by the rightward axial jet with many tiny bubbles fragmented by the instability along the boundaries of the axial jet and the outer expanding fronts of B_1 (also see the 30 ms picture).

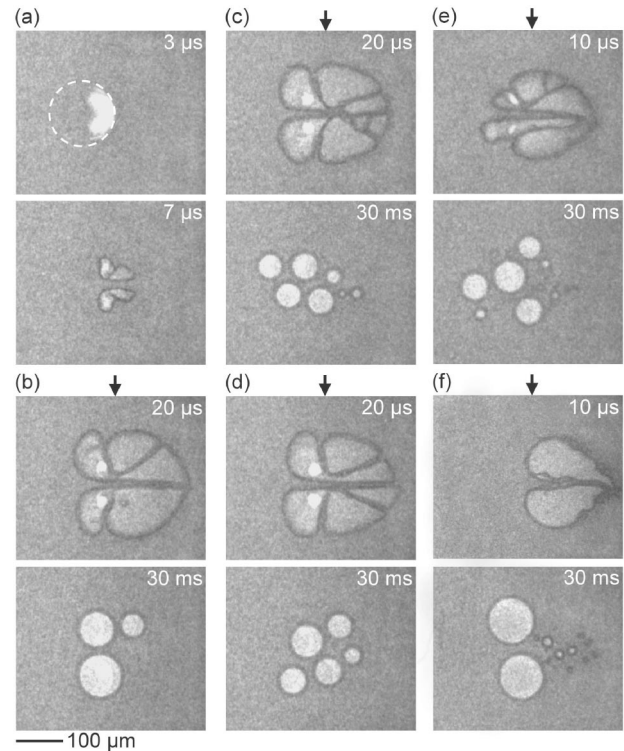


FIG. 4. (a) The typical patterns of B_1 at the compression and the initial reexpansion stage at $E_1 = 220 \mu\text{J}$, $E_2 = 105 \mu\text{J}$, and $D_L = 500 \mu\text{m}$. The dashed circle corresponds to the initial boundary of B_1 . (b), (c), (d) Three different sets of typical intermediate states for B_1 at stage II ($t = 20 \mu\text{s}$) and the corresponding final states (30 ms) induced by the unstable transverse jet under the same operating conditions as (a). (e) The more complicated intermediated and final configuration under stronger shock by shortening D_L to $350 \mu\text{m}$. (f) The fragmentation pattern of B_1 with suppressed leftward expansion by increasing E_2 to $140 \mu\text{J}$ while increasing D_L back to $500 \mu\text{m}$. The arrows indicate the initial right edge of B_1 .

Using a simplified picture, the two interacting bubbles are somehow similar to two coupled and damped oscillators. The coupling strength increases with the decreasing D_L . When B_2 expands, the energy can be transferred to B_1 through the flow field. The interplay with the inertia causes the over-compression and the subsequent rebounding of B_1 . The work done by B_2 on B_1 in the initial stage makes the maximum volume and the time for reaching the maximum volume of B_2 smaller than those in the absence of B_1 [Fig. 3(a)]. The hydrodynamic interaction with B_1 also makes the B_2 shape noncircular. In stage I, after the shock reaches B_1 , the collapsing of B_1 with rightward jetting induces easier rightward advancing of the liquid between B_1 and B_2 , and the faster expansion of the right edge of B_2 than of its rest part, which elongates B_2 . Figure 5 shows that at small $D_L (= 200 \mu\text{m})$, and E_1 and $E_2 = 220$ and $90 \mu\text{J}$ respectively, the right pole of B_2 becomes pointed and even entrains the indented part (rightward jetting) of B_1 as it collapses. In stage II, the reflected pressure wave

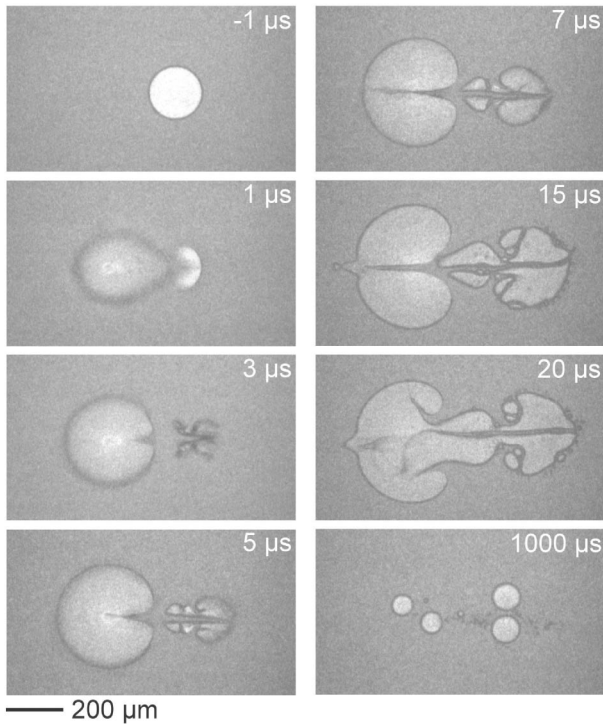


FIG. 5. The sequential snapshots of the bubble configuration at $E_1 = 220 \mu\text{J}$, $E_2 = 90 \mu\text{J}$ and $D_L = 200 \mu\text{m}$, showing the strong backward interaction from B_1 to B_2 and their strong entanglement at low D_L .

from the rebounding B_1 first retards and flattens the expanding right edge of B_2 but not the left edge (see the runs from 8 to 20 μs in Fig. 2). It further causes the indentation and the subsequent formation of a leftward jet at smaller D_L (Fig. 5). Unlike in the case of large D_L (Fig. 2), the left part of B_1 (left to the necking) has a higher expansion rate associated with the leftward jetting of B_2 (Fig. 5). The latter entrains the leftward jet and eventually merges with B_1 . The strong mutual interaction at shorter D_L but lower E_2 also induces unstable fragmentation process and makes the configuration of final bubbles asymmetric and not reproducible.

The above alternate opposite jetting and entrainment phenomenon has also been observed in an expanding and then collapsing bubble near a free surface [7]. Namely, to B_2 , the left edge of B_1 plays a role similar to the free surface. In our case, the pressure built up in B_1 in its compression stage further speeds up its later rebounding and enhances the backward jetting of B_2 with B_1 entrainment. We also observe the formation of a cusp interface but without the penetration jet on B_1 at large D_L (not shown). Note that no multiple reflection of the pressure wave between the two bubbles has been observed under all the tested conditions.

In conclusion, we have demonstrated the detailed dynamical evolution of the interaction between a laser in-

duced bubble B_1 and another nearby bubble B_2 by a subsequent laser pulse in a thin ink between two glass slices. The background flow field mediates the complemented anisotropic expanding-contracting processes of the two adjacent bubbles. The field associated with the sudden finite expansion of B_2 anisotropically compresses B_1 and generates a forward axial jet. In the following early reexpanding stage of B_1 , the jet protruding through the opposite edge of B_1 with gas entraining, and the transverse jet induced necking under the nonuniform surrounding pressure field cause the formation of butterfly-shaped two side lobes. The unstable transverse jetting caused by increasing E_2 or decreasing D_L leads to the asymmetric fragmentation of B_1 into many final small bubbles. The expanding part left to the necking can be fully eliminated at large E_2 . Tiny bubbles are generated by the strong flow in the central axial jet and the outer expanding front of B_1 . The backward interaction from B_1 first induces elongation or even entrainment of B_2 into the collapsing B_1 in the early expanding stage of B_2 and then induces a backward indentation or jetting in its later collapsing stage. At small D_L , the strong interaction merges the two bubbles and induces complicated entangled intermediate patterns and asymmetric fragmentation.

This work is supported by the National Science Council of the Republic of China under Contract No. NSC93-2112-M008-019.

-
- [1] For example, A. Walton and G. Reynolds, *Adv. Phys.* **33**, 595 (1984); C.E. Brennen, *Cavitation and Bubble Dynamics* (Oxford University Press, New York, 1995).
 - [2] For example, M. Borghesi *et al.*, *Phys. Rev. Lett.* **88**, 135002 (2002); H. Y. Chu, Y. K. Chiu, C. L. Chan, and Lin I, *Phys. Rev. Lett.* **90**, 075004 (2003).
 - [3] M. Versluis *et al.*, *Science* **289**, 2114 (2000).
 - [4] O. Baghdassarian *et al.*, *Phys. Rev. Lett.* **86**, 4934 (2001); C. D. Ohl, O. Lindau, and W. Lauterborn, *Phys. Rev. Lett.* **80**, 393 (1998).
 - [5] M. S. Plesset and R. B. Chapman, *J. Fluid Mech.* **47**, 283 (1971).
 - [6] E. A. Brujan, G. S. Keen, A. Vogel, and J. R. Blake, *Phys. Fluids* **14**, 85 (2002).
 - [7] R. B. Robinson *et al.*, *J. Appl. Phys.* **89**, 8225 (2001).
 - [8] F. P. Bowden, F. R. S. Brunton, and J. H. Brunton, *Proc. R. Soc. A* **236**, 433 (1960); J. P. Dear, J. E. Field, and A. J. Walton, *Nature (London)* **332**, 505 (1988).
 - [9] C. D. Ohl and R. Ikink, *Phys. Rev. Lett.* **90**, 214502 (2003).
 - [10] K. O. Greulich *et al.*, *J. Microsc.* **198**, 182 (2000).
 - [11] V. Venugopalan *et al.*, *Phys. Rev. Lett.* **88**, 078103 (2002).
 - [12] R. Richtmyer, *Commun. Pure Appl. Math.* **13**, 297 (1960); E. Meshkov, *Fluid Dyn.* **4**, 101 (1972); G. Jourdan and L. Houas, *Phys. Fluids* **8**, 1353 (1996).
 - [13] B. Dersten, C. D. Ohl, and A. Prosperetti, *Phys. Fluids* **15**, 821 (2003).